Molecular Vision 2017; 23:8-19 <http://www.molvis.org/molvis/v23/8>
Received 11 May 2016 | Accepted 26 January 2017 | Published 28 January 2017

Mertk gene expression and photoreceptor outer segment phagocytosis by cultured rat bone marrow mesenchymal stem cells

Rong-mei Peng,[1] Jing Hong,[1] Ying Jin,[1] Yu-zhao Sun,[2] Yi-qian Sun,[1] Pei Zhang[1]

[1]Department of Ophthalmology, Peking University Third Hospital, Beijing, China Key Laboratory of Vision Loss and Restoration, Ministry of Education, Beijing, China; [2]Department of Ophthalmology, China Medical University, the First Affiliated Hospital, Shenyang, China

Background: Bone marrow mesenchymal stem cells (BM-MSCs) are multipotential stem cells that have been used for a broad spectrum of indications. Several investigations have used BM-MSCs to promote photoreceptor survival and suggested that BM-MSCs are a potential source of cell replacement therapy for some forms of retinal degeneration.
Purpose: To investigate the expression of the MER proto-oncogene*, tyrosine kinase (Mertk)*, involved in the disruption of RPE phagocytosis and the onset of autosomal recessive retinitis pigmentosa in rat BM-MSCs and to compare phagocytosis of the photoreceptor outer segment (POS) by BM-MSCs and RPE cells in vitro.
Methods: MSCs were isolated from the bone marrow of Brown Norway rats. Reverse transcription-PCR (RT–PCR) and western blot analyses were used to examine the expression of *Mertk*. The phagocytized POS was detected with double fluorescent labeling, transmission electron microscopy, and scanning electron microscopy.
Results: *Mertk* expression did not differ among the first three passages of BM-MSCs. *Mertk gene* expression was greater in the BM-MSCs than the RPE cells. Mertk protein expression in the BM-MSCs was similar to that in the RPE cells in the primary passage and was greater than that in the RPE cells in the other two passages. BM-MSCs at the first three passages phagocytized the POS more strongly than the RPE cells. The process of BM-MSC phagocytosis was similar to that of the RPE cells.
Conclusions: BM-MSCs may be an effective cell source for treating retinal degeneration in terms of phagocytosis of the POS.

Photoreceptor outer segment (POS) phagocytosis is a key function of RPE cells in supporting photoreceptors [1]. Defects in POS phagocytosis can lead to photoreceptor degeneration, such as retinitis pigmentosa (RP) and age-related macular degeneration (AMD), which leads to permanent visual loss in humans [2]. The most effective treatment is autologous RPE transplantation [3]. However, obtaining an intact RPE sheet and transplanting it to the lesion area is complicated. Obtaining an RPE sheet damages an area of the healthy retinal structure, which limits the number of RPE cells on the sheet. It is important to find a source of replacement cells.

Bone marrow mesenchymal stem cells (BM-MSCs) can be aspirated directly from donors and cultured for ex vivo expansion. The cells are multipotent and have low immunogenicity, so they can be used for a broad range of indications. MSCs can differentiate into bone, cartilage, skeletal muscle, endothelium, cardiac muscle, and hepatocytes in vitro and in vivo [4-10]. In addition, the cells can differentiate into RPE or retinal cells ex vivo [11]. Subretinal injection of MSCs has also been reported to induce differentiation into photoreceptor cells in a sodium iodate–induced retinal degeneration rat model [12]. BM-MSCs were injected into the subretina or through the vein in Royal College of Surgeons (RCS) rats or a retinal trauma rat model that delayed retinal degeneration and preserved retinal function [13]. Furthermore, studies based on paracrine effects hypothesize that MSCs can secrete neurotrophic factors to protect against photoreceptor degeneration in different animal models [14-18]. To date, there are three ongoing registered clinical trials using MSCs on RP (NCT01531348; NCT01920867; NCT01914913) and two on AMD (NCT01920867; NCT02016508). Results from these studies have not been reported yet.

The role of RPE cells in phagocytosis involves multiple steps, including the binding, uptake, and degradation of engulfed POS. The MER proto-oncogene, *tyrosine kinase* (*MERTK,* Gene ID 10461, OMIM 604705), a member of the MER/AXL/TYRO3 receptor kinase family and expressed in the RPE, is involved in POS ingestion [19]. Mutations in *MERTK* are known to cause retinal pigmentosa [20,21].

Correspondence to: Jing Hong, Peking University Third Hospital, Peking University Eye Center, No.49 Garden North Road, Haidian, Beijing, China, 100191; Phone: 00 86-010-8226-6566; FAX: 00 86-010-8208-9951; email: hongjing64@yahoo.com

Previously, some studies activated or blocked *MERTK* to enhance or inhibit the RPE phagocytosis of POS, respectively [22,23]. *MERTK* is an essential component of the signaling network that controls phagocytosis in RPE, the loss of which results in photoreceptor degeneration [24]. In this study, we compared BM-MSCs and RPE cells in terms of *Mertk* expression and involvement in phagocytosis in vitro.

METHODS

BM-MSC culture: This research followed the tenets of the Declaration of Helsinki and was approved by the Institutional Review Committee at Peking University Third Hospital. The animals were handled according to the Association for Research in Vision and Ophthalmology (ARVO) Statement for the Use of Animals in Ophthalmic and Vision Research. All procedures were approved by Peking University's Institutional Animal Care and Use Committee. BM-MSCs were isolated from Brown Norway (BN) rats weighing 150–200 g (Vital River, Beijing, China). Briefly, the rats were killed with cervical dislocation. The femurs and tibias were dissected and cleaned of all soft tissue. The epiphysis was clipped. Bone marrow was obtained by flushing the femurs and tibias with complete medium consisting of Dulbecco's Modified Eagle Medium- low glucose (DMEM-LG, Gibco, CA), 10% fetal bovine serum (FBS, Gibco-Invitrogen), and 100 units/ml penicillin/streptomycin (Sigma, St. Louis, MO). The cells were cultured in a humidified incubator at 37 °C and 5% CO_2 for 48 h. Non-adherent cells were removed with three washes with 1× PBS (1X; 137 mM NaCl, 2.7 mM KCl, 10 mM Na_2HPO_4, 2 mM KH_2PO_4, pH 7.4). The adherent cells were further cultured in complete medium replaced every 2 days. Once the adherent cells were grown to 80% confluence, they were detached with 0.25% trypsin-EDTA (Sigma) and replated at a 1:3 dilution under the same culture conditions. The cells were expanded by several passages. The isolated cells were confirmed to differentiate into osteoblasts and adipocytes with alizarin red staining and Oil Red O staining, respectively. The primary passage was recorded as P_0, the second passage as P_1, and the third passage as P_2.

RPE cell culture: Rat RPE cells were harvested from the BN rats. The eyeballs were dissected after the femurs and tibias were dissected. The eyes were incubated with 20 ml PBS containing tobramycin 20 mg for 20 min three times and rinsed with PBS. The anterior segments (the cornea, iris epithelium, and crystalline lens), the vitreous, and the neural retina were removed. The remaining tissue was incubated in 0.25% trypsin-EDTA for 30 min at 37 °C, and the RPE cells were detached from the choroid with the use of a 1 ml pipette. The dissociated cells were centrifuged at 107 ×g for 8 min at 4 °C. The RPE cells were resuspended with complete DMEM/F-12 (Gibco-Invitrogen) medium containing 10% FBS and 100 units/ml penicillin/streptomycin and seeded into 35 mm^2 culture dishes (Corning, Inc., Corning, NY). The RPE cells at 80% confluence were passaged at a 1:3 dilution.

RT–PCR: Total RNA from the P_0, P_1, and P_2 rat BM-MSCs and RPE cells was prepared with RNAiso Plus (D9108A, Takara Bio, Inc., Shiga, Japan) in accordance with the manufacturer's instructions and quantified on a spectrophotometer (Thermo Scientific, Wilmington, DE) for standardization with the equation optical density (OD) 260 × 40 × dilution ratio/1,000. Reverse transcription was performed according to the manufacturer's instructions (PrimeScript RT Master Mix, Takara Bio) to generate total cDNA with a thermocycler (T-Gradient Thermoblock, Biometra,Goettingen, Germany). Real-time PCR involved the relative quantification protocol on an ABI 7500 system (Applied Biosystems, Foster City, CA) with the primers for rat *Mertk* (forward) 5′-TCG GAA TGA GAT TGG CTG GTC-3′ and (reverse) 5′-AAT TGG AGG CTT CGT CCA TCT G-3′ (148 bp); and β-actin (forward) 5′-TGT TGC CCT AGA CTT CGA GCA-3′ and (reverse) 5′-GGA CCC AGG AAG GAA GGC T-3′ (153 bp; the primers were designed by Takara Bio). The cDNA was diluted at 1:5 with RNAase-free water. cDNA was amplified in a 10 µl mixture containing 5 µl Premix Ex, 0.2 µl Mertk/β-actin forward primer (10 µmol/l), 0.2 µl Mertk/β-actin reverse primer (10 µmol/l), 0.2 µl ROX Reference Dye II (50×), and 1 µl cDNA template, according to the manufacturer's protocol (SYBR Premix Ex Taq II [Perfect Real Time], Takara Bio). The cycle conditions were 95 °C for 1 min and 95 °C for 30 s, followed by 40 cycles of 5 s at 95 °C and 34 s at 60 °C. β-actin quantification was used as an internal control for normalization. In addition, a no-template control (ddH_2O) was analyzed for each template. The relative difference in gene expression was analyzed with the $2^{-\Delta\Delta CT}$ method [25]. An expression ratio >2 designated upregulation, 0.5–2 the same expression, and <0.5 downregulation.

Western blot analysis: The P_0, P_1, and P_2 rat BM-MSCs and RPE cells were lysed with 1× cell signaling lysis buffer [26]. The cell lysates were centrifuged at 4 °C at 13800 ×g. The protein concentrations were determined with the Bicinchoninic Acid Protein Assay Kit (Pierce, Rockford, IL) with bovine serum albumin (BSA) as a standard. Western blot analysis was performed according to standard procedures. Proteins were resolved on sodium dodecyl sulfate–polyacrylamide gel electrophoresis (SDS–PAGE) and transferred to polyvinylidene difluoride (PVDF) membranes (Millipore, Millipore, MA), which were blocked for 2 h with 5% skim milk and incubated for 24 h with the primary polyclonal

antibodies for Mertk (C-term)-Aff-Purified (AP10151PU-N; Acris antibodies, Germany) and β-actin (sc-130657; Santa Cruz Biotechnology, Santa Cruz, CA) at 4 °C, then with horseradish peroxidase-conjugated secondary antibodies (sc-2301; Santa Cruz Biotechnology), and developed with an enhanced chemiluminescent substrate or SuperSignal West Femto Maximum Sensitivity Substrate (Pierce).

Immunocytochemistry: Cells were washed three times with PBS and fixed with 4% paraformaldehyde for 15 min at 4 °C, blocked in 10% goat serum for 30 min, then incubated with primary antibody diluted in 0.5% BSA at 37 °C for 2 h, washed three times with PBS, and incubated with secondary antibodies for 45 min at 37 °C. Nuclei were stained with 4',6-diamidino-2-phenylindole (DAPI, 1:5,000; Sigma, Aldrich). The stained samples were visualized with fluorescence microscopy (Nikon,Tokyo, Japan) and quantified by using Image Pro Plus 5.0 (Media Cybernetics, Bethesda, MD). At least three independent experiments were performed in duplicate.

Osteogenic and adipogenic differentiation in vitro:

Osteogenic differentiation—A total of 3×10^3/well P_2 BM-MSCs were cultured in six-well plates for osteogenic differentiation. The cells were treated with osteogenic medium for 3 weeks. The medium was changed every 3 days. The osteogenic medium contained DMEM-LG (Gibco) supplemented with 10% FBS, 50 µg/ml ascorbate-2 phosphate, 10^{-8} M dexamethasone, and 10 mM β-glycerophosphate (all Sigma, St. Louis, MO). The calcified nodules were identified with alizarin red staining.

Adipogenic differentiation—A total of 2×10^4/well P2 BM-MSCs were cultured in six-well plates for adipogenic differentiation. The BM-MSCs were treated with adipogenic medium for 3 weeks. The adipogenic medium contained DMEM-LG supplemented with 10% FBS, 50 µg/ml ascorbate-2 phosphate, 10^{-7} M dexamethasone, 10 µg/ml insulin, and 50 µg/ml indomethacin (Sigma). For evaluation of the adipocytes, the cells were fixed with 4% formaldehyde and stained with Oil Red O (Sigma).

Preparation of rat POS: The POS was isolated from the BN rats as described [27]. Briefly, the retina tissue was suspended in a sucrose-homogenizing medium containing 34% sucrose (w/w), 65 mM NaCl, 2 mM $MgCl_2$, and 5 mM Tris-acetate buffer (pH 7.4). The density of the solution was slightly greater than 1.15 g/ml. In total, 20 retinas were homogenized in 15 ml medium by shaking vigorously for 1 min. This procedure sheared off most of the POS at the junction of the inner and outer segments. The POS was then partially separated from the remainder of the retina and sedimented at 427 ×g at 4 °C for 4 min. The suspended POS in the supernatant was decanted into two volumes of 10 mM Tris-acetate (pH 7.4), and the pellet was resuspended in fresh homogenizing medium and rehomogenized with a homogenizer. This gentle shearing force released the POS (approximately 15%) into the supernatant after repeated centrifugation at 427 ×g. Then the diluting supernatant was centrifuged at 427 ×g for 4 min. The resulting pellets (the crude POS) were resuspended in 25% sucrose medium containing 1 mM $MgCl_2$ and 10 mM Tris-acetate (pH 7.4). The resuspended crude POS was rehomogenized with a 26-g syringe. This step sheared the crude POS into small fragments. The rehomogenized POS was layered on top of a discontinuous gradient buffered with 10 mM Tris-acetate (pH 7.4) and containing 1 mM $MgCl_2$ and sucrose in incremental density steps of 1.15, 1.13, and 1.10 g/ml. The gradients were centrifuged at 135173 ×g for 30 min. The floccules between the densities of 1.10 and 1.13 g/ml were collected (the refined POS) and stained as described [28]. The isolated POS was incubated with DMEM containing 10 µg/ml fluorescein isothiocyanate (FITC) for 1 h at room temperature. Then the FITC-stained POS (FITC-POS) was pelleted with microcentrifugation (4 min at 4000 ×g), resuspended in growth medium, counted, and diluted to a final concentration of 10^7/ml.

Double fluorescent vital assay of phagocytosis: A double fluorescent vital assay of phagocytosis was developed to detect the function of the MSC and RPE cells phagocytizing the POS and latex beads according to a protocol modified from Margaret J. McLaren [29]. The details are as follows.

POS phagocytosis: Daily phagocytosis of the POS is one of the critical and specific functions of RPE cells. In this study, POS phagocytosis was compared between MSCs and RPE cells. The BM-MSCs and the RPE cells were cultured on 1 cm^2 coverslips. For staining, the cells were cultured for 36 h in growth medium containing sulforhodamine (SR) at a final concentration of 40 µg/ml. The SR-containing medium was removed 12 h before the addition of the rods. The BM-MSCs and the RPE cells were overlaid with the prepared FITC-POS and incubated at 37 °C. One coverslip was taken out of the Petri dishes at chase intervals (incubated with the FITC-POS for 1, 3, 6, 9, 12, 24, 30, 36, and 48 h), rinsed free of the unattached FITC-POS, and fixed with 2% paraformaldehyde in 0.1 mol/l phosphate buffer (pH 7.4). Nuclei were stained with DAPI (1:5,000).

Latex bead phagocytosis: Latex bead phagocytosis is non-specific. The cells were incubated for 36 h in growth medium containing FITC at a final concentration of 10 µg/ml. The FITC-containing medium was removed, and a final

concentration of 10^7/ml, latex bead culture medium was added. After incubation, the coverslips were washed with PBS to remove unbound latex beads. Cells were fixed and stained with DAPI.

Quantitation: Bound and ingested POS and latex beads were quantified manually from the pictures. At least five different areas of each plate were quantified with three independent experiments performed repeatedly.

Scanning electron microscopy: Cells grown on 25 mm^2 coverslips were incubated with 10^7/ml POS medium for 3 or 24 h. The coverslips were washed with PBS to remove the unbound POS, and the cells were fixed in 3% glutaraldehyde in PBS for 2 h at room temperature, washed three times with PBS, and then dehydrated through a graded series of ethanol, 30%, 50%, 70%, 80%, 90%, and twice at 100%, for 20 min each. Samples were critical-point-dried, sputter-coated with 20 nm gold-palladium, and examined with scanning electron microscopy (SEM; JSM-5600LV; JEOL, Tokyo, Japan).

Transmission electron microscopy: Cells were incubated with 10^7/ml POS medium for 24 and 48 h, washed with PBS to remove the unbound POS, and scraped with a cell scraper. Samples were centrifuged at 800 ×g for 8 min; the supernatant was removed, fixed with 3% glutaraldehyde for 1 h at room temperature with new 3% glutaraldehyde once, postfixed with 1% osmium tetroxide, washed three times in PBS for 5 min each, then dehydrated through a graded series of ethanol, and embedded in Epon 812. Ultrathin (80 nm) sections were collected on copper grids and double-stained with uranyl acetate and lead citrate and then examined with transmission electron microscopy (TEM; JEM-1230; JEOL).

Statistical analysis: Data are expressed as mean ± standard deviation (SD) and were analyzed with one-way ANOVA. A p value of less than 0.05 was considered statistically significant. Analysis involved the use of SPSS 16.0 (SPSS Inc., Chicago, IL).

RESULTS

Characterization of rat BM-MSCs: Rat BM-MSCs can be successfully isolated and cultured in a whole bone-marrow adherent culture system. Primary BM-MSCs showed nest-like growth with a homogenous, fibroblast-like morphology in the first three passages (Appendix 1). The BM-MSCs were positive for CD44 and CD90 (Appendix 1) and negative for CD34 and CD45 and differentiated into adipocytes and osteoblasts (Appendix 1).

Characterization of rat RPE cells: Primary rat RPE cells were cultured successfully and showed the typical polygonal morphology and abundant pigment granules (Appendix 2). The cell morphology changed during the following passages (Appendix 2). The appearance of cells was fibroblast-like, with fewer pigment granules. The granules were lost from the cells and diluted by cell division. The RPE cells were positive for RPE65, CK3, and S-100 according to immunofluorescence (Appendix 2).

Mertk expression in rat BM-MSCs and RPE cells: Compared with the RPE cells, the expression of the *Mertk gene* of rat BM-MSCs was upregulated at the same passage with real-time PCR (as shown in Figure 1 in the first three columns). The *Mertk gene* expression of the BM-MSCs was greater than that of the RPE cells, especially at P_0 and P_1 (as shown in Figure 1 in the first two columns).The *Mertk gene* expression among the first three passages showed no difference (as shown in Figure 1 in the last two columns).

Figure 2 shows the Mertk protein expression. Quantitative western blot analysis showed the following: Mertk protein expression in the RPE P_0 was significantly greater than that in the RPE P_1 ($p = 0.02$), but there was no difference with the RPE P_2 ($p = 0.124$). There was no difference between the RPE P_1 and the RPE P_2 ($p = 0.353$); Mertk protein expression in the MSC P_0 was lower than in the MSC P_1 ($p = 0.005$) and P_2 ($p = 0.000$), with no difference between the MSC P_1 and P_2 ($p = 0.62$). Mertk protein expression in the MSC P_0 was not different from that in the RPE P_0 ($p = 0.388$) but was statistically significant greater than in the RPE in other two passages ($p = 0.000$).

Phagocytosis function:

Double fluorescent vital assay of phagocytosis—Latex bead phagocytosis is shown in Figure 3. Under fluorescent microscopy, the latex beads exhibited red fluorescence. The cells that was incubated in FITC exhibited green fluorescence. If the latex beads were phagocytized by the cells, the beads were yellow. POS phagocytosis is shown in Figure 4 and Appendix 3. Under fluorescent microscopy, the POS exhibited green fluorescence. The cells incubated in SR exhibited red fluorescence. If the POS was phagocytized by the cells, it was yellow. The quantity of the phagocytized latex beads and POS by the BM-MSCs and the RPE cells is shown in Figure 5. The quantity of phagocytized latex beads did not differ between the BM-MSCs and the RPE cells from 3 to 18 h ($p>0.05$) but differed at other time points ($p<0.05$). The quantity of phagocytized POS differed between the BM-MSCs and the RPE cells except at 3 h ($p = 0.49$). Before 3 h, phagocytic ability was stronger for the RPE cells than for the BM-MSCs. After that, the situation was the reverse. However, the phagocytic ability was due to the cell vigor.

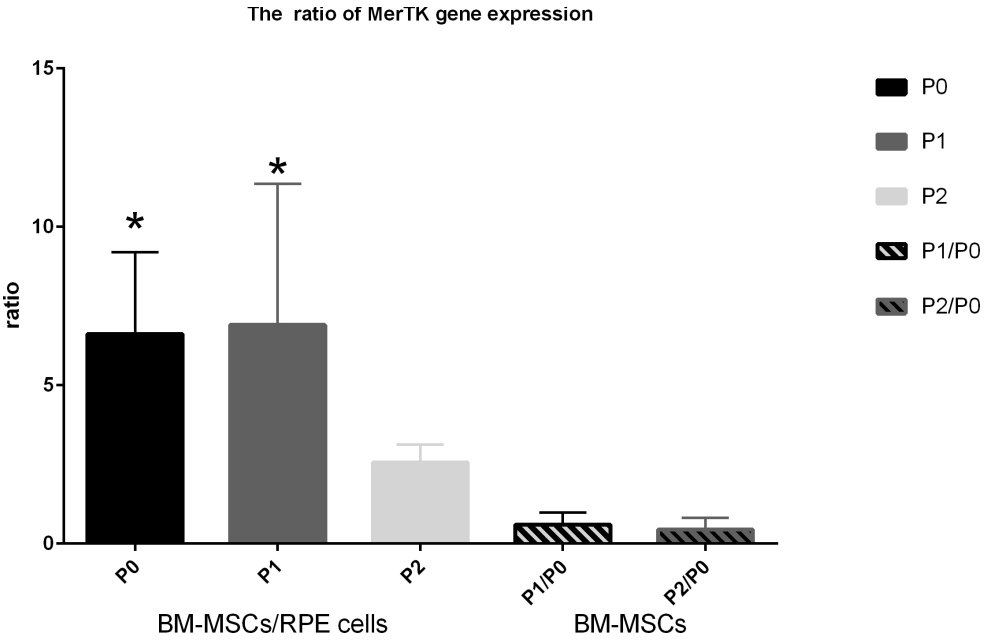

Figure 1. The MER proto-oncogene and the *Mertk gene* expression ratio between BM-MSCs and RPE cells at different passages and among different passages of BM-MSCs. The first three columns show the ratio of bone marrow mesenchymal stem cells (BM-MSCs) versus RPE cells. The last two columns show the ratio among different passages of BM-MSCs. The asterisk (*) represents $p<0.05$. The sampling size for each group is 3.The error bars are standard deviation (SD). The data were analyzed with one-way ANOVA. The *Mertk* gene expression of BM-MSCs was significant greater than RPE cells at P0 and P1.

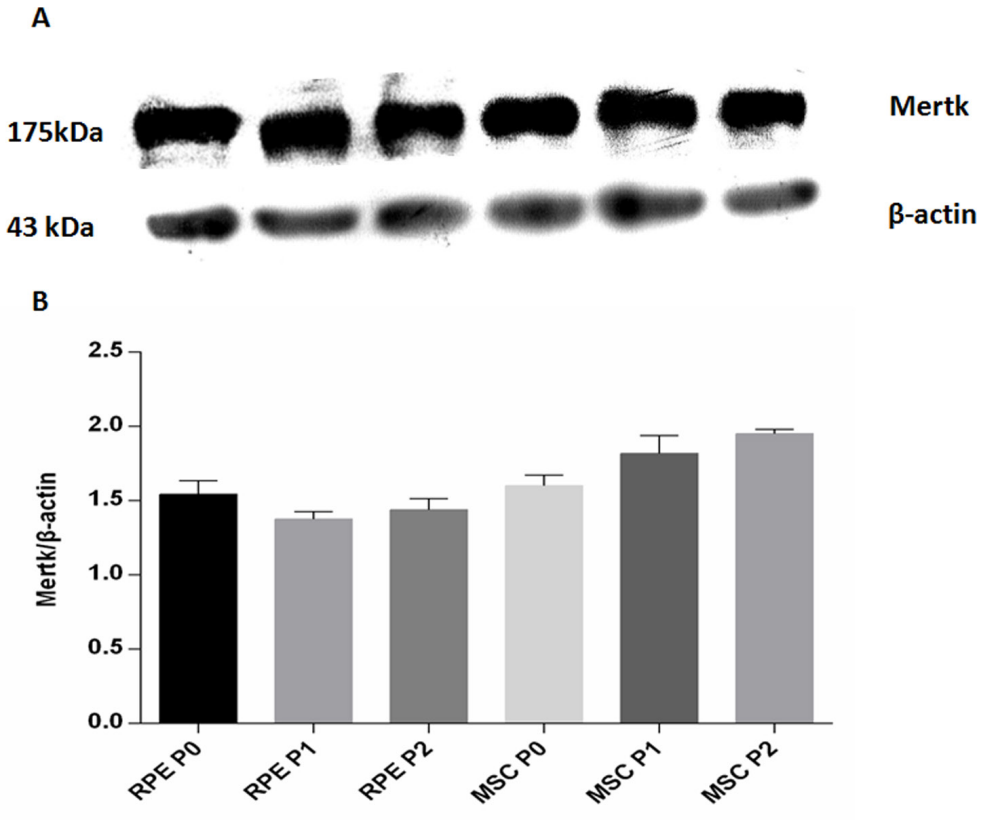

Figure 2. Western blot analysis of Mertk protein expression in different passages of RPE cells and BM-MSCs. **A**: Upper panel, Mertk protein expression. Lower panel, protein samples assayed for β-actin expression, control for protein loading. **B**: Quantification of Mertk protein expression. The sampling size for each group is 3.The error bars are standard deviation (SD). The data were analyzed with one-way ANOVA. Mertk protein expression in RPE P0 was significantly greater than in RPE P1. Mertk protein expression in MSC P0 was lower than MSC P1. Mertk protein expression in MSC P1 and P2 was significant greater than RPE.

Because the cells were in the mitotic stage, they could phagocytize more granules.

Ultrastructure of BM-MSCs and RPE cells during POS phagocytosis: SEM showed that the BM-MSCs and the RPE cells had microvilli on the surface (Figure 6, the filled white arrows). The POS bound to the cell surface (Figure 6, the empty white arrows). The cytomembrane around the POS changed, and endocytosis was activated. TEM showed the internal structure of the phagocytized POS by the BM-MSCs and RPE cells (Figure 7). Many vesicles named phagolysosomes were found in the cytoplasm. The layer-like substance in the vesicles was the phagocytized POS. The POS in the vesicles was smaller at 48 h than 24 h which meant the POS was digested. There was more fluid in the vesicles at 48 h than at 24 h.

DISCUSSION

RPE cells are crucial to maintain visual function as a metabolic gatekeeper. Among their many functions, the ability to ingest and degrade the POS is important for photoreceptor survival [30]. The phagocytic dysfunction of RPE cells leads to many fundus diseases, such as age-related macular degeneration. Here, we compared phagocytosis of the RPE POS by RPE cells and rat BM-MSCs, as an alternative to RPE cells, in vitro, for treating RPE-related retinopathy. We also examined the expression of *Mertk*, involved in disruption of RPE phagocytosis and the onset of autosomal recessive retinitis pigmentosa in BM-MSCs and RPE cells. *Mertk* expression did not differ among the first three passages of the BM-MSCs but was greater in the BM-MSCs than in the RPE cells. Mertk protein expression in the BM-MSCs was similar to that in the RPE cells in the primary passage and was greater than that in the RPE cells in the other two passages. The BM-MSCs at the

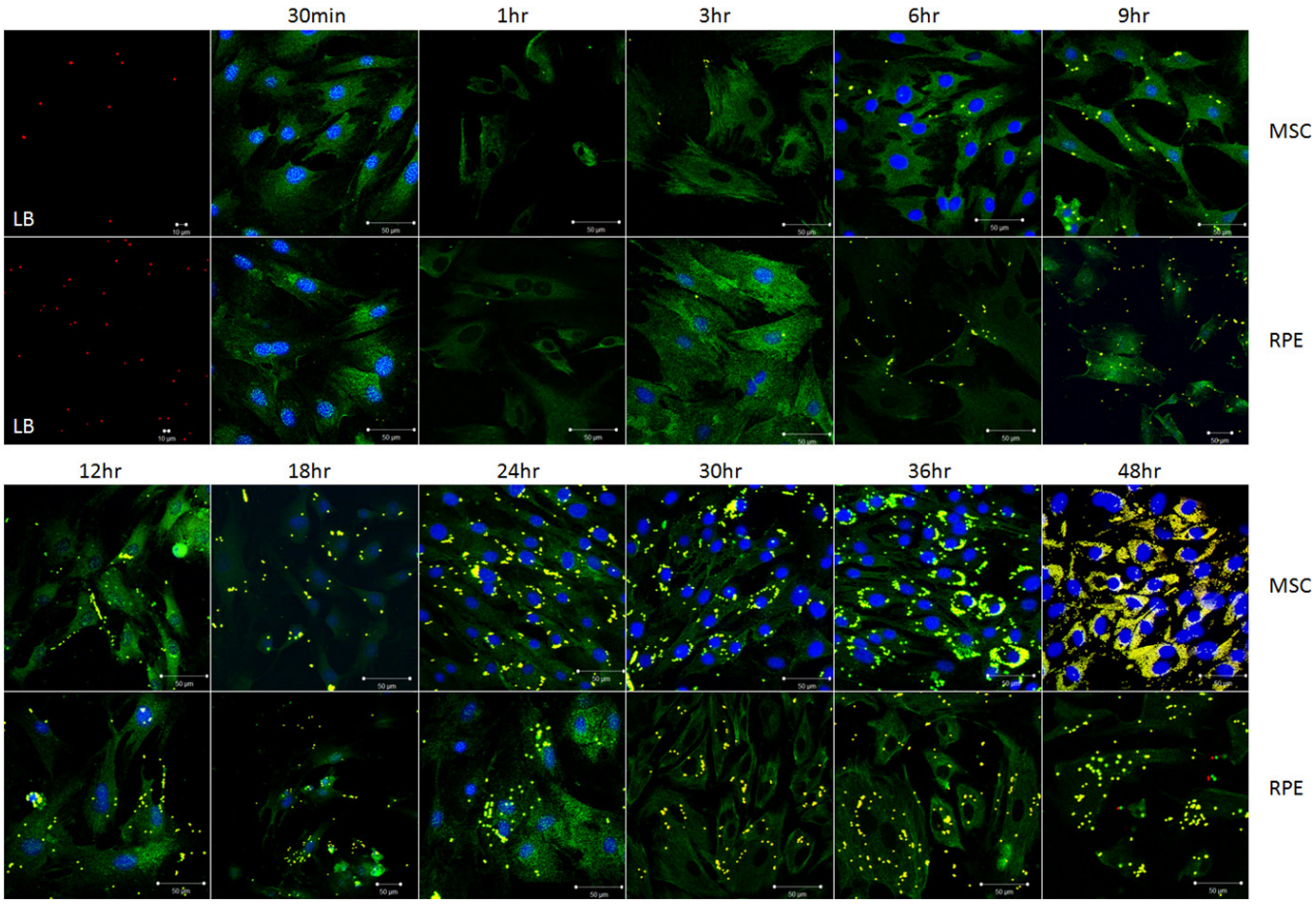

Figure 3. Latex beads phagocytosis by BM-MSCs and RPE cells. The first picture in rows 1 and 2 exhibits latex beads by fluorescent microscopy magnified 200X and 400X, respectively. Rows 1 and 3 show bone marrow mesenchymal stem cells (BM-MSCs) incubated with LBs for different time periods. Rows 2 and 4 show RPE cells incubated with LBs for different time periods. The latex beads phagocytized by cells are yellow. LB = latex beads.

first three passages phagocytized the POS and more strongly than the RPE cells. The process of BM-MSC phagocytosis was similar to that of the RPE cells in digesting the POS. BM-MSCs may be an effective cell source for treating retinal degeneration.

We have many methods for treating RPE dysfunction-related retinopathy, including gene therapy [31], antivascular endothelial growth factor (VEGF) agents [32], photodynamic therapy, angiostatic steroids, and an artificial retina [33]. All these methods have defects; for example, with anti-VEGF agents, the effective time is limited, and the injection often needs to be repeated [32,34]. With cytotherapy to treat RPE-related retinopathy, including RPE transplantation and stem cell therapy, RPE sheets could be autologous or allogeneic. The success rate of allogeneic RPE sheet transplantation is low because of strong rejection. The effect of autologous RPE sheet transplantation is better than that of allogeneic transplantation, but the cell numbers are limited, which damages a healthy peripheral area of the eye [35]. Therefore, if possible, stem cell transplantation is a better choice. MSCs can be conveniently obtained from different accessible tissues: bone marrow, blood, and adipose and dental tissue. MSCs were originally identified in the bone marrow, representing 0.001–0.01% of the bone marrow population. The advantages of MSCs include high proliferative and differentiation abilities, neuroprotective effects, paracrine effects, and strong immunosuppressive properties, making MSCs an attractive therapeutic tool, although transient rash, self-limiting bacterial infections, or fever might occur in some patients after MSC transplantation [36-38].

The RPE cell phagocytic process involves multiple steps, including the binding, uptake, and degradation of

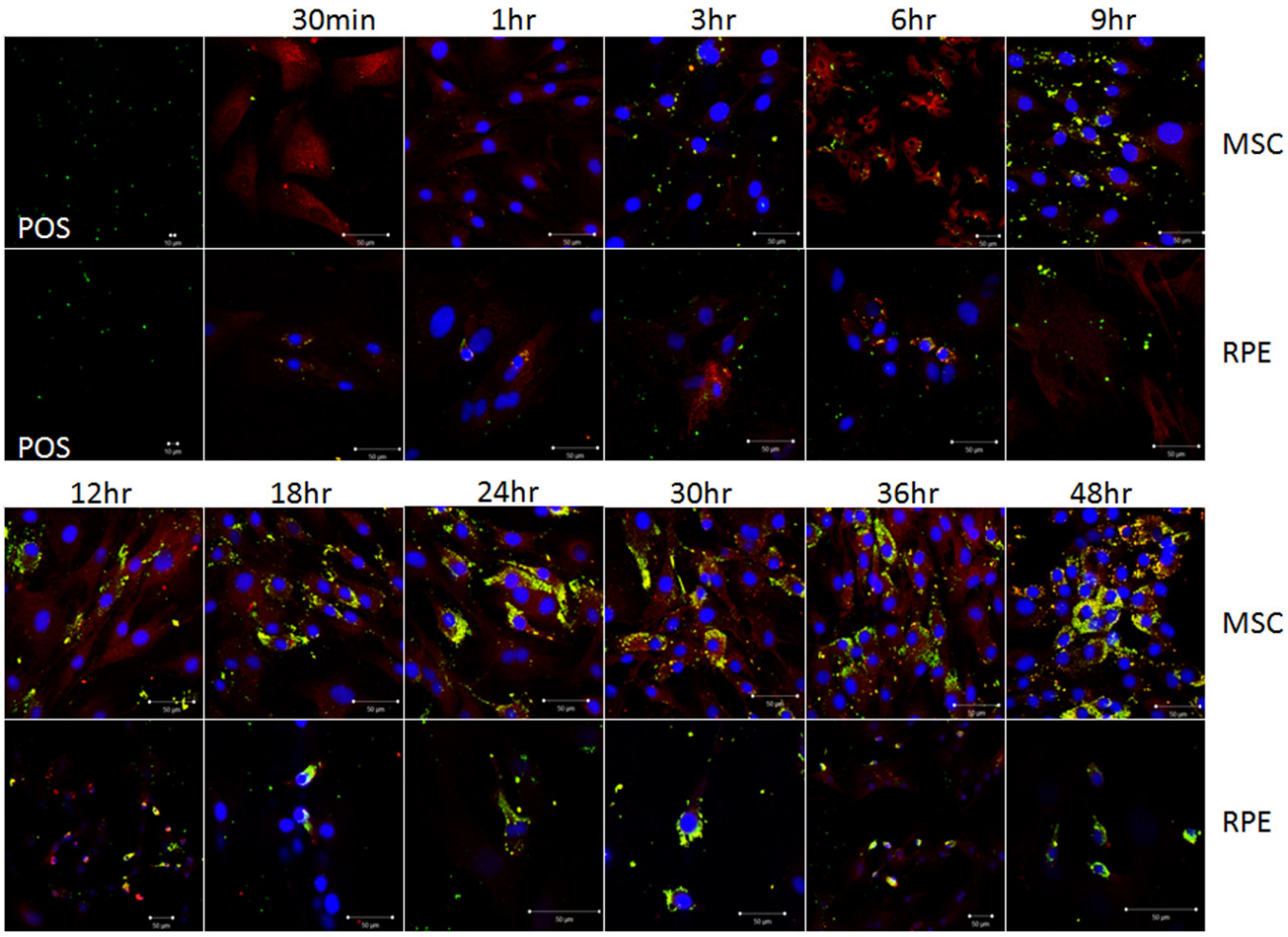

Figure 4. POS phagocytosis by BM-MSCs and RPE cells. The first picture in rows 1 and 2 exhibits the photoreceptor outer segment (POS) with fluorescent microscopy magnified 200X and 400X, respectively. Rows 1 and 3 show bone marrow mesenchymal stem cells (BM-MSCs) incubated with the POS for different time periods. Rows 2 and 4 show RPE cells incubated with the POS for different time periods. The POS phagocytized by the cells is yellow.

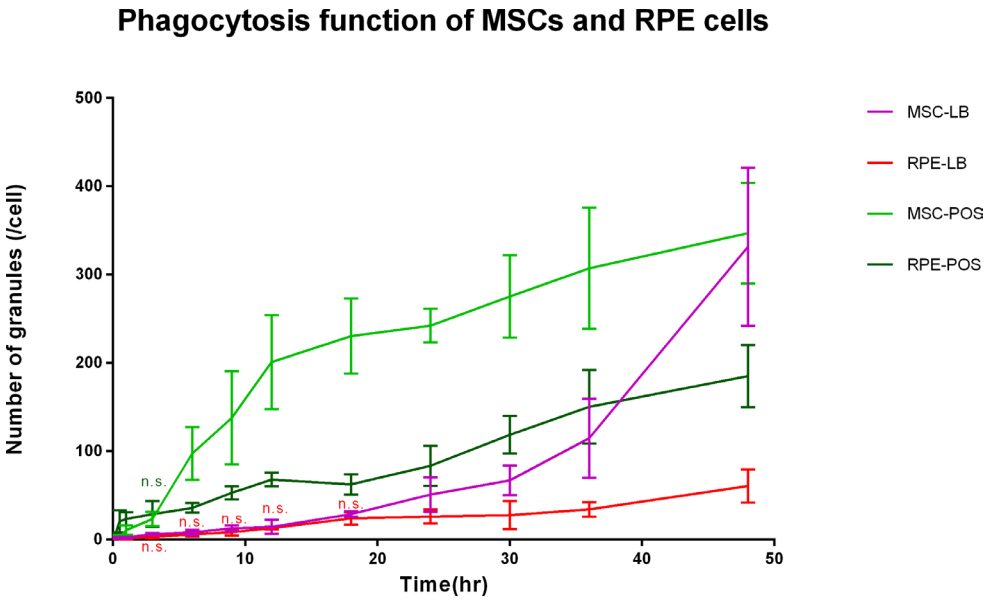

Figure 5. Quantity of phagocytic latex beads (LBs) and photoreceptor outer segment (POS) by bone marrow mesenchymal stem cells (BM-MSCs) and RPE cells incubated with LB and POS for different time periods. n.s. means no statistical significance between the BM-MSCs and the RPE cells. The sampling size for each group is 3.The error bars are standard deviation (SD). The data were analyzed with one-way ANOVA. The quantity of phagocytized latex beads did not differ between the BM-MSCs and the RPE cells from 3 to 18 h ($p>0.05$) but differed at other time points ($p<0.05$). The quantity of phagocytized POS differed between the BM-MSCs and the RPE cells except at 3 h ($p = 0.49$). Before 3 h, phagocytic ability was stronger for the RPE cells than for the BM-MSCs. After that, the situation was the reverse.

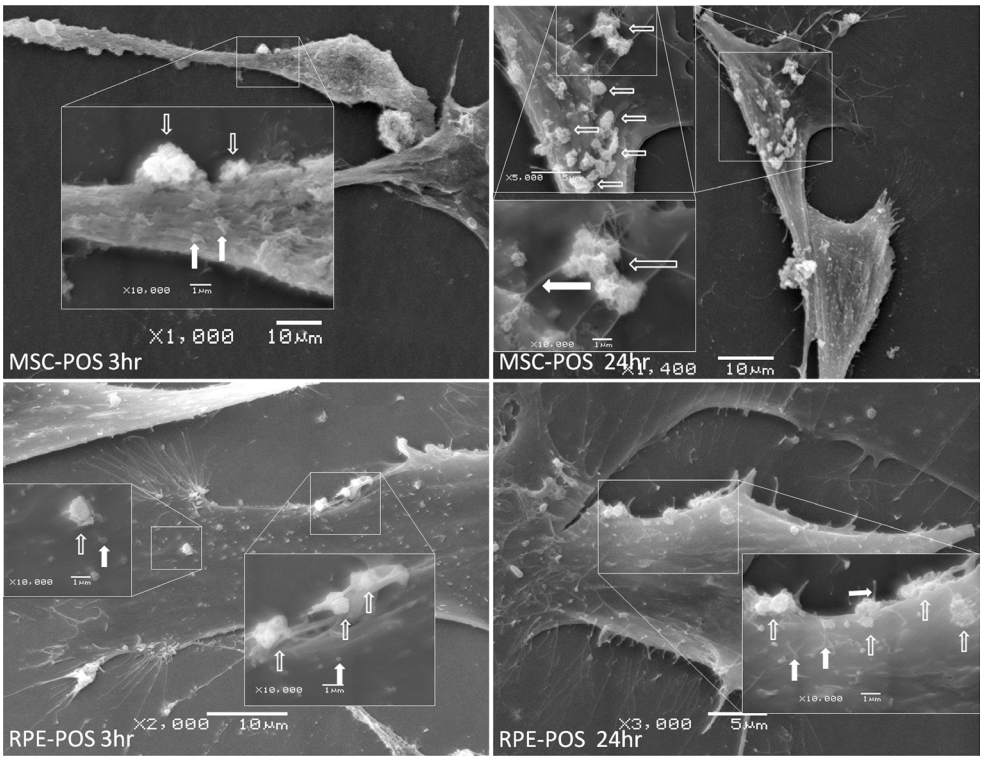

Figure 6. The exterior structure of BM-MSC and RPE cell phagocytic activity on scanning electron microscopy. (Top left) Bone marrow mesenchymal stem cells (BM-MSCs) were incubated with the photoreceptor outer segment (POS) for 3 h. (Top right) BM-MSCs were incubated with the POS for 24 h. (Bottom left) RPE cells were incubated with the POS for 3 h. (Bottom right) RPE cells were incubated with the POS for 24 h. The empty white arrows indicate the POS that bound to the cell surface. The filled white arrows indicate microvilli. The common point of the MSC and RPE cells is the cytomembrane that protrudes around the bound POS.

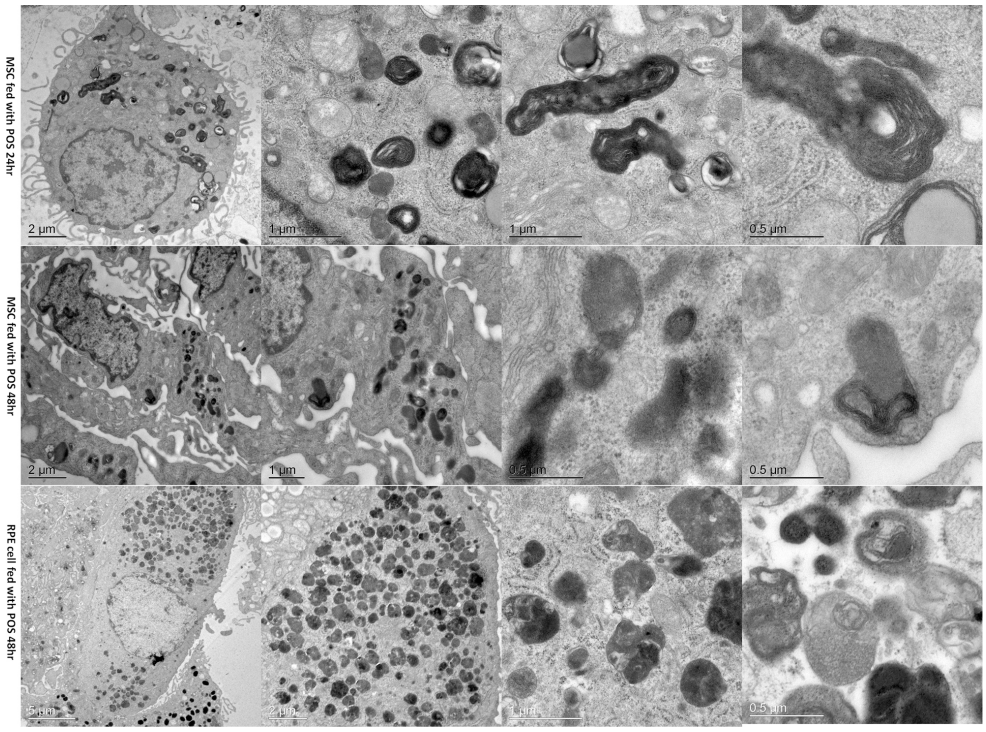

Figure 7. The internal structure of BM-MSC and RPE cell phagocytic activity on transmission electron microscopy. (Row 1) Bone marrow mesenchymal stem cells (BM-MSCs) phagocytizing the photoreceptor outer segment (POS) at 24 h at different magnifications. (Row 2) BM-MSCs phagocytizing POS for 48 h. The layer-like substance was smaller than at 24 h. (Row 3) RPE cells phagocytizing the POS for 48 h. The layer-like substance was less and more loose at 48 h than at 24 h.

the engulfed POS. The vitronectin receptor αvβ5 [39] and a class B scavenger receptor, CD36 [40], are two known RPE cell-surface receptors involved in POS binding. POS binding to the αvβ5 receptor mobilizes the focal adhesion kinase (FAK). FAK plays an important role in the transmission of αvβ5-induced cytoplasmic signals and the reorganization of the actin cytoskeleton during POS phagocytosis. FAK causes redistribution of Mertk [41]. Mertk leads to POS ingestion [42]. After being engulfed by RPE cells, the POS is digested by lysosomal enzymes, with opsin mainly digested by cathepsin D, an acidic lysosomal protease, and the waste products released into the choroidal circulation.

In this study, the rat BM-MSCs possessed a specific and nonspecific phagocytic ability similar to that of the RPE cells. In the specific phagocytosis assay, the POS phagocytic ability of the BM-MSCs and the RPE cells was nearly the same during the first 3 h, but 3 h later, the BM-MSCs showed stronger specific phagocytic ability than that of the RPE cells, and the difference increased with time, up to 48 h, the end of the observation, to the maximum difference. In nonspecific phagocytosis, the performance of the BM-MSCs was later than that in specific phagocytosis and was the same as that of the RPE cells within 18 h. However, the BM-MSCs had stronger phagocytic ability than the RPE cells 18 h later, which continued to the end of the experiment. The BM-MSCs and the RPE cells had identical phagocytic processes, in terms of the binding, uptake, or degradation of the engulfed POS, as seen on SEM and TEM; the quantity of POS was higher in the BM-MSCs than in the RPE cells, which indicates stronger phagocytosis ability.

This stronger phagocytosis ability for BM-MSCs than for RPE cells was confirmed with the gene and protein expression of Mertk. Real-time PCR findings suggested that the Mertk expression of P_0–P_2 BM-MSCs was similar, but the quantity in the RPE cells was reduced with the passages. The expression was greater in the BM-MSCs than the RPE cells. In addition, western blot suggested that Mertk expression of MSCs was stronger than that of RPE cells in the P1 and the P2. Thus, the BM-MSCs possessed similar ability to or even stronger ability than RPE cells to ingest the POS.

The MERTK protein is a member of the Axl/Mer/Tyro3 receptor tyrosine kinase family and is expressed in RPE cells leading to POS ingestion [43,44]. *Mertk* is the gene mutated in the RCS rat, a well-studied animal model of retinal degeneration [45]. Therefore, BM-MSCs possessing the POS phagocytosis ability may explain why photoreceptor apoptosis was inhibited after the BM-MSCs were injected in the subretina or through the vein in the RCS rats or the retinal trauma rat model [13]. The RPE cells of the RCS rats lose the ability for phagocytosis of the POS, thus leading to POS accumulation and photoreceptor apoptosis. A substitute that can perform the function of RPE cells (phagocytosis and metabolism of

the POS) could aid in photoreceptor survival. In the present study, the BM-MSCs strongly expressed Mertk, which is significant in digesting the POS, and adhered to, engulfed, and digested the POS. Therefore, BM-MSCs may be a good alternative to RPE cells. In conclusion, BM-MSCs possess some of the RPE cell ability for phagocytosis of the POS and may be potential seed cells to treat RPE-related retinopathy. An animal study to determine whether BM-MSCs have the same function by implanting an MSC sheet in the subretinal cavity in RCS rats.

APPENDIX 1.

To access the data, click or select the words "Appendix 1." Morphology and identification of rat bone-marrow mesenchymal stem cells (BM-MSCs). (A) primary BM-MSCs (P0) were cultured for 3 days. The cells grew in a nest shape. The center of the nest was the germinal center. The cells were fibroblast-like. (B) Primary BM-MSCs were cultured for 6 days. The number of cells increased. (C, D) Second-passage (P1) and third-passage (P2) cells. The cell morphology was not changed. (E, F) BM-MSCs were positive for CD44 and CD90 by immunofluorescence. Cells were homogenous, fibroblast-like during the first 3 passages. (G) Fat particles of differentiated adipocytes were stained red with Oil-red O (Methylene blue couterstaining, original magnification 1000×). (H) Calcified nodules of differentiated osteoblasts were stained with Alizarin red.

APPENDIX 2.

To access the data, click or select the words "Appendix 2." Morphology and identification of rat retinal pigment epithelium (RPE) cells. (A) Primary RPE cells (P0) were polygonal and contained abundant pigment granules. (B) Second-passage (P1) RPE cells were fibroblast-like. The pigment granules were less than at P0. (C) Third-passage RPE cells contained few pigment granules. (D) RPE cells were positive for CK3 by immunofluorescence. One cell contained pigment granules (arrow). (E, F) RPE cells were positive for RPE65 and S-100 by immunofluorescence.

APPENDIX 3.

To access the data, click or select the words "Appendix 3." Photoreceptor outer segment (POS) phagocytosis by BM-MSCs and RPE cells (100× magnification). Rows 1 and 3 show BM-MSCs and rows 2 and 4 show RPE cells incubated with POS for different time.

ACKNOWLEDGMENTS

Funding/Support: grants from the National Natural Science Foundation of China (No.30871315, No. 31140025 and No. 31271045) and National Basic Research Program of China (973 Program; No. 2011CB510200).

REFERENCES

1. Simo R, Villarroel M, Corraliza L, Hernandez C, Garcia-Ramirez M. The retinal pigment epithelium: something more than a constituent of the blood-retinal barrier–implications for the pathogenesis of diabetic retinopathy. J Biomed Biotechnol 2010; xxx:190724-.
2. Zobor D, Zrenner E. Retinitis pigmentosa - a review. Pathogenesis, guidelines for diagnostics and perspectives. Ophthalmologe 2012; 109:501-14. , 515. [PMID: 22581051].
3. Han L, Ma Z, Wang C, Dou H, Hu Y, Feng X, Xu Y, Yin Z, Wang X. Autologous transplantation of simple retinal pigment epithelium sheet for massive submacular hemorrhage associated with pigment epithelium detachment. Invest Ophthalmol Vis Sci 2013; 54:4956-63. [PMID: 23744996].
4. Komatsu K, Honmou O, Suzuki J, Houkin K, Hamada H, Kocsis JD. Therapeutic time window of mesenchymal stem cells derived from bone marrow after cerebral ischemia. Brain Res 2010; 1334:84-92. [PMID: 20382136].
5. Heng BC, Saxena P, Fussenegger M. Heterogeneity of baseline neural marker expression by undifferentiated mesenchymal stem cells may be correlated to donor age. J Biotechnol 2014; 174C:29-33. [PMID: 24486027].
6. Holmes B, Castro NJ, Li J, Keidar M, Zhang LG. Enhanced human bone marrow mesenchymal stem cell functions in novel 3D cartilage scaffolds with hydrogen treated multi-walled carbon nanotubes. Nanotechnology 2013; 24:365102-[PMID: 23959974].
7. Huang CC, Tsai HW, Lee WY, Lin WW, Chen DY, Hung YW, Chen JW, Hwang SM, Chang Y, Sung HW. A translational approach in using cell sheet fragments of autologous bone marrow-derived mesenchymal stem cells for cellular cardiomyoplasty in a porcine model. Biomaterials 2013; 34:4582-91. [PMID: 23528228].
8. Ding L, Zhu H, Yang Y, Wang ZD, Zheng XL, Yan HM, Dong L, Zhang HH, Han DM, Xue M, Liu J, Zhu L, Guo ZK, Wang HX. Functional mesenchymal stem cells remain present in bone marrow microenvironment of patients with leukemia post-allogeneic hematopoietic stem cell transplant. Leuk Lymphoma 2014; [PMID: 24180332].
9. Bukulmez H, Bilgin A, Caplan AI, Jones O. A112: Prevention of Late Stage Renal Failure in BXSB SLE Mouse Model with Human Bone Marrow Derived Mesenchymal Stem Cell Treatment. Arthritis Rheumatol 2014; 66:Suppl 11S149-.
10. Nagaishi K, Ataka K, Echizen E, Arimura Y, Fujimiya M. Mesenchymal stem cell therapy ameliorates diabetic hepatocyte damage in mice by inhibiting infiltration of bone

marrow-derived cells. Hepatology 2014; 59:1816-29. [PMID: 24375439].

11. Huang C, Zhang J, Ao M, Li Y, Zhang C, Xu Y, Li X, Wang W. Combination of retinal pigment epithelium cell-conditioned medium and photoreceptor outer segments stimulate mesenchymal stem cell differentiation toward a functional retinal pigment epithelium cell phenotype. J Cell Biochem 2012; 113:590-8. [PMID: 21948619].
12. Huo DM, Dong FT, Yu WH, Gao F. Differentiation of mesenchymal stem cell in the microenviroment of retinitis pigmentosa. Int J Ophthalmol 2010; 3:216-9. [PMID: 22553557].
13. Zhang Y, Wang W. Effects of bone marrow mesenchymal stem cell transplantation on light-damaged retina. Invest Ophthalmol Vis Sci 2010; 51:3742-8. [PMID: 20207980].
14. Tassoni A, Gutteridge A, Barber AC, Osborne A, Martin KR. Molecular Mechanisms Mediating Retinal Reactive Gliosis Following Bone Marrow Mesenchymal Stem Cell Transplantation. Stem Cells 2015; 33:3006-16. [PMID: 26175331].
15. Junyi L, Na L, Yan J. Mesenchymal stem cells secrete brain-derived neurotrophic factor and promote retinal ganglion cell survival after traumatic optic neuropathy. J Craniofac Surg 2015; 26:548-52. [PMID: 25723663].
16. Dreixler JC, Poston JN, Balyasnikova I, Shaikh AR, Tupper KY, Conway S, Boddapati V, Marcet MM, Lesniak MS, Roth S. Delayed administration of bone marrow mesenchymal stem cell conditioned medium significantly improves outcome after retinal ischemia in rats. Invest Ophthalmol Vis Sci 2014; 55:3785-96. [PMID: 24699381].
17. Johnson TV, DeKorver NW, Levasseur VA, Osborne A, Tassoni A, Lorber B, Heller JP, Villasmil R, Bull ND, Martin KR, Tomarev SI. Identification of retinal ganglion cell neuroprotection conferred by platelet-derived growth factor through analysis of the mesenchymal stem cell secretome. Brain 2014; 137:503-19. [PMID: 24176979].
18. Zhang Y, Wang W. Effects of bone marrow mesenchymal stem cell transplantation on light-damaged retina. Invest Ophthalmol Vis Sci 2010; 51:3742-8. [PMID: 20207980].
19. Feng W, Yasumura D, Matthes MT, LaVail MM, Vollrath D. Mertk triggers uptake of photoreceptor outer segments during phagocytosis by cultured retinal pigment epithelial cells. J Biol Chem 2002; 277:17016-22. [PMID: 11861639].
20. Abu-Safieh L, Alrashed M, Anazi S, Alkuraya H, Khan AO, Al-Owain M, Al-Zahrani J, Al-Abdi L, Hashem M, Al-Tarimi S, Sebai MA, Shamia A, Ray-Zack MD, Nassan M, Al-Hassnan ZN, Rahbeeni Z, Waheeb S, Alkharashi A, Abboud E, Al-Hazzaa SA, Alkuraya FS. Autozygome-guided exome sequencing in retinal dystrophy patients reveals pathogenetic mutations and novel candidate disease genes. Genome Res 2013; 23:236-47. [PMID: 23105016].
21. Ostergaard E, Duno M, Batbayli M, Vilhelmsen K, Rosenberg T. A novel MERTK deletion is a common founder mutation in the Faroe Islands and is responsible for a high proportion of retinitis pigmentosa cases. Mol Vis 2011; 17:1485-92. [PMID: 21677792].
22. Murase H, Tsuruma K, Shimazawa M, Hara H. TUDCA Promotes Phagocytosis by Retinal Pigment Epithelium via MerTK Activation. Invest Ophthalmol Vis Sci 2015; 56:2511-8. [PMID: 25804419].
23. Qin S. Blockade of MerTK Activation by AMPK Inhibits RPE Cell Phagocytosis. Adv Exp Med Biol 2016; 854:773-8. [PMID: 26427488].
24. Ghazi NG, Abboud EB, Nowilaty SR, Alkuraya H, Alhommadi A, Cai H, Hou R, Deng WT, Boye SL, Almaghamsi A, Al Saikhan F, Al-Dhibi H, Birch D, Chung C, Colak D, LaVail MM, Vollrath D, Erger K, Wang W, Conlon T, Zhang K, Hauswirth W, Alkuraya FS. Treatment of retinitis pigmentosa due to MERTK mutations by ocular subretinal injection of adeno-associated virus gene vector: results of a phase I trial. Hum Genet 2016; [PMID: 26825853].
25. Livak KJ, Schmittgen TD. Analysis of relative gene expression data using real-time quantitative PCR and the 2(-Delta Delta C(T)) Method. METHODS 2001; 25:402-8. [PMID: 11846609].
26. Zhang H, Feng H, Luo L, Zhou Q, Luo Z, Peng Y. Distinct effects of knocking down MEK1 and MEK2 on replication of herpes simplex virus type 2. Virus Res 2010; 150:22-7. [PMID: 20172001].
27. Papermaster DS. Preparation of retinal rod outer segments. Methods Enzymol 1982; 81:48-52. [PMID: 6212746].
28. McLaren MJ, Inana G, Li CY. Double fluorescent vital assay of phagocytosis by cultured retinal pigment epithelial cells. Invest Ophthalmol Vis Sci 1993; 34:317-26. [PMID: 7680023].
29. McLaren MJ, Inana G, Li CY. Double fluorescent vital assay of phagocytosis by cultured retinal pigment epithelial cells. Invest Ophthalmol Vis Sci 1993; 34:317-26. [PMID: 7680023].
30. Young RW. The renewal of photoreceptor cell outer segments. J Cell Biol 1967; 33:61-72. [PMID: 6033942].
31. Abedi F, Wickremasinghe S, Richardson AJ, Makalic E, Schmidt DF, Sandhu SS, Baird PN, Guymer RH. Variants in the VEGFA gene and treatment outcome after anti-VEGF treatment for neovascular age-related macular degeneration. Ophthalmology 2013; 120:115-21. [PMID: 23149126].
32. Lad EM, Hammill BG, Qualls LG, Wang F, Cousins SW, Curtis LH. Anti-VEGF treatment patterns for neovascular age-related macular degeneration among medicare beneficiaries. Am J Ophthalmol 2014; 158:537-43. [PMID: 24857687].
33. Lorach H, Benosman R, Marre O, Ieng SH, Sahel JA, Picaud S. Artificial retina: the multichannel processing of the mammalian retina achieved with a neuromorphic asynchronous light acquisition device. J Neural Eng 2012; 9:66004-[PMID: 23075696].
34. Brown DM, Chen E, Mariani A, Major JJ. Super-dose anti-VEGF (SAVE) trial: 2.0 mg intravitreal ranibizumab for recalcitrant neovascular macular degeneration-primary end point. Ophthalmology 2013; 120:349-54. [PMID: 23131717].

35. Da CL, Chen FK, Ahmado A, Greenwood J, Coffey P. RPE transplantation and its role in retinal disease. Prog Retin Eye Res 2007; 26:598-635. [PMID: 17920328].

36. Aoki H, Hara A, Nakagawa S, Motohashi T, Hirano M, Takahashi Y, Kunisada T. Embryonic stem cells that differentiate into RPE cell precursors in vitro develop into RPE cell monolayers in vivo. Exp Eye Res 2006; 82:265-74. [PMID: 16150443].

37. Lu B, Malcuit C, Wang S, Girman S, Francis P, Lemieux L, Lanza R, Lund R. Long-term safety and function of RPE from human embryonic stem cells in preclinical models of macular degeneration. Stem Cells 2009; 27:2126-35. [PMID: 19521979].

38. Stanzel BV, Liu Z, Somboonthanakij S, Wongsawad W, Brinken R, Eter N, Corneo B, Holz FG, Temple S, Stern JH, Blenkinsop TA. Human RPE stem cells grown into polarized RPE monolayers on a polyester matrix are maintained after grafting into rabbit subretinal space. Stem Cell Rep 2014; 2:64-77. [PMID: 24511471].

39. Nandrot EF. Animal Models, in "The Quest to Decipher RPE Phagocytosis". Adv Exp Med Biol 2014; 801:77-83. [PMID: 24664683].

40. Sun M, Finnemann SC, Febbraio M, Shan L, Annangudi SP, Podrez EA, Hoppe G, Darrow R, Organisciak DT, Salomon RG, Silverstein RL, Hazen SL. Light-induced oxidation of photoreceptor outer segment phospholipids generates ligands for CD36-mediated phagocytosis by retinal pigment epithelium: a potential mechanism for modulating outer segment phagocytosis under oxidant stress conditions. J Biol Chem 2006; 281:4222-30. [PMID: 16354659].

41. Finnemann SC. Focal adhesion kinase signaling promotes phagocytosis of integrin-bound photoreceptors. EMBO J 2003; 22:4143-54. [PMID: 12912913].

42. Nandrot EF, Dufour EM. Mertk in daily retinal phagocytosis: a history in the making. Adv Exp Med Biol 2010; 664:133-40. [PMID: 20238011].

43. Shelby SJ, Colwill K, Dhe-Paganon S, Pawson T, Thompson DA. MERTK interactions with SH2-domain proteins in the retinal pigment epithelium. PLoS One 2013; 8:e53964- [PMID: 23390493].

44. Conlon TJ, Deng WT, Erger K, Cossette T, Pang JJ, Ryals R, Clement N, Cleaver B, McDoom I, Boye SE, Peden MC, Sherwood MB, Abernathy CR, Alkuraya FS, Boye SL, Hauswirth WW. Preclinical potency and safety studies of an AAV2-mediated gene therapy vector for the treatment of MERTK associated retinitis pigmentosa. Hum Gene Ther Clin Dev 2013; 24:23-8. [PMID: 23692380].

45. Deng WT, Dinculescu A, Li Q, Boye SL, Li J, Gorbatyuk MS, Pang J, Chiodo VA, Matthes MT, Yasumura D, Liu L, Alkuraya FS, Zhang K, Vollrath D, LaVail MM, Hauswirth WW. Tyrosine-mutant AAV8 delivery of human MERTK provides long-term retinal preservation in RCS rats. Invest Ophthalmol Vis Sci 2012; 53:1895-904. [PMID: 22408006].

Articles are provided courtesy of Emory University and the Zhongshan Ophthalmic Center, Sun Yat-sen University, P.R. China. The print version of this article was created on 28 January 2017. This reflects all typographical corrections and errata to the article through that date. Details of any changes may be found in the online version of the article.